Interface resistance and transparency in ferromagnet/superconductor Co/Nb_xTi_{1-x} multilayers ($x=1$, 0.6, and 0.4)

S.-Y. Huang,[1,2] S. F. Lee,[1,*] S. Y. Hsu,[2] and Y. D. Yao[1]
[1]*Institute of Physics, Academia Sinica, Taipei, Taiwan 115, Republic of China*
[2]*Institute of Electrophysics, National Chaio-Tung University, Hsinchu, Taiwan 300, Republic of China*
(Received 16 January 2007; revised manuscript received 1 May 2007; published 27 July 2007)

The quantitative interface resistance between polycrystalline ferromagnetic Co and Nb_xTi_{1-x}, with $x=1$, 0.6, and 0.4, is measured and analyzed at 4.2 K. Both the superconducting and normal states of Nb_xTi_{1-x}, respectively, above and below the superconducting critical thickness, are studied with current flowing perpendicular to the interface. A one-band series-resistance model is used to analyze our data. The interface transparencies in terms of the ratio between interface resistance and various physical quantities are discussed.

DOI: 10.1103/PhysRevB.76.024521 PACS number(s): 74.45.+c, 72.15.−v, 73.40.−c, 74.78.Fk

I. INTRODUCTION

The rich physics of interplay between ferromagnetism and superconductivity has recently attracted much theoretical and experimental attention (see Refs. 1 and 2 as reviews). The interest continues due to the progress in the preparation of both new materials and high quality heterostructures down to nanometer size. Singlet superconductivity prefers an antiparallel spin orientation of electrons to form Cooper pairs, while ferromagnetic order forces the spins to align in parallel. In artificially fabricated layered systems, the proximity effect between superconductor (S) and normal metal (NM) manifests itself as exponentially decaying amplitude of the superconducting Cooper pairs wave function, which penetrates across the interface into NM.[3] On the other hand, in a ferromagnet/superconductor (F/S) junction, the superconducting Cooper pair wave function extends from superconductor into ferromagnet with damped oscillatory behavior due to the exchange field in F. The coherence length of the pair wave function in F, which determines the oscillation length and the penetration depth in F, is given by $\xi_F^{\mathrm{ex}}=\frac{\hbar v_F}{2E_{\mathrm{ex}}}$ in the clean limit, and $\xi_F^{\mathrm{ex}}=\sqrt{\frac{\hbar D_F}{2E_{\mathrm{ex}}}}$ in the dirty limit, where D_F is the diffusion constant, v_F is the Fermi velocity, and l_F is the mean free path in F.[2,4] The properties of superconducting wave functions under the influence of exchange field can be studied by changing the relative strengths of the two competing orderings.

There is much evidence of the pairing amplitude oscillation. For instance, Kontos *et al.*[5] observed spatial oscillations of the electron density of state for different thickness of ferromagnets from tunneling spectroscopy. Radovic *et al.*[6] predicted nonmonotonic dependence of the critical temperature of F/S bilayers and multilayers on ferromagnet layer thickness and it was observed experimentally in Ni/Nb bilayers,[7] Gd/Nb,[8] Co/Nb, and Co/V multilayers.[9,10] Jiang *et al.* attributed the oscillation to the π phase in Gd/Nb multilayers, but Mühge *et al.*[11] pointed out that the magnetic dead layers played a dominant role in similar oscillation behavior in Fe/Nb/Fe trilayers.

It is considered as an unambiguous proof of π-phase shift when measurements of the formation of metallic Josephson junctions with ferromagnetic barriers ($S/F/S$) were reported. Such π junctions have been characterized as having nonmonotonic behavior of the critical current as functions of temperature[12] and ferromagnetic thickness.[13] Weak ferromagnetic layers of Cu_xNi_{1-x} were essential to achieve appropriate exchange energy in a suitable window of experimental phase space. These phenomena mentioned above were related to the interaction between superconductivity and magnetism and occurred around the boundary of the F/S structures. The coexistence of superconductivity and magnetic order has been studied for several decades. Fulde and Ferrell[14] and Larkin and Ovchinnikov[15] theoretically demonstrated that superconductivity and ferromagnetism may coexist (FFLO state) in bulk materials. It meant that nonzero total momentum pairing could occur when an exchange field E_{ex} was present in the F/S layer structure. In order to study the transport properties, it is important to understand which boundary condition is applicable at the interfaces. It is common to find discussions in the literature that treats interfacial transparency in terms of the ratio of interface resistance to the product of bulk resistivity and the Cooper pair penetration depth in the NM.[16–21] Studies on $V/V_{1-x}Fe_x$ ($x=1-0.34$) multilayers were performed with current in-plane measurements to discuss and derive different interface transparency from theoretical fitting.[21] The imperfection of the interface in the real system plays an important role. However, there are few experiments which directly and systematically investigate the influence of interface resistance on the interfacial transparency between S and F, both when S is in the normal state and in the superconducting state. In this paper, we report our experimental results on the resistance of F/S multilayer systems using a strong ferromagnet Co with current perpendicular to plane (CPP) measurement in the diffusive regime. Quantitative analysis of the unit area interface resistance between F and S, both in the superconducting state and in the normal state by varying the S thickness, is presented. Since the interface resistance must be considered as areas conduct in parallel, the unit area resistance we are interested in is AR, total sample area multiplied by the sample resistance. Furthermore, we compare the unit area interface resistance of the F/S system and analyze the influence of interface transparency with three superconductors, Nb, $Nb_{0.6}Ti_{0.4}$, and $Nb_{0.4}Ti_{0.6}$. The paper is organized as follows. In Sec. II we introduce the sample fabrication and measure-

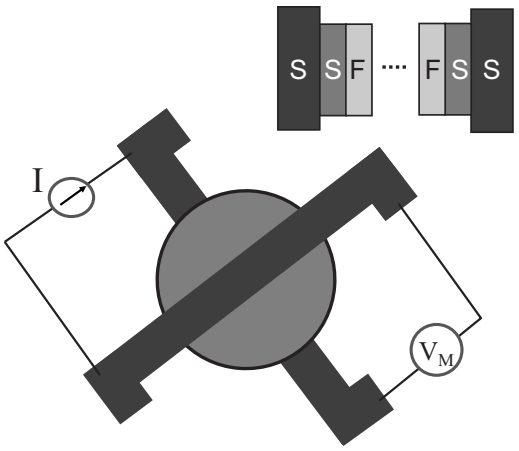

FIG. 1. Schematic drawing of sample for current-perpendicular-to-plane resistance measurement. The middle part is the multilayer of interest. The drawing is not to scale.

ments. In Sec. III we describe the results of our CPP data and the fitting procedures by one-band model. In Sec. IV we discuss and compare the interface resistances from our quantitative CPP analysis. Finally, in Sec. V we summarize our work.

II. CPP SAMPLE FABRICATION AND MEASUREMENTS

A. Sample preparation

We fabricated several series of Co/Nb, Co/$Nb_{0.6}Ti_{0.4}$, and Co/$Nb_{0.4}Ti_{0.6}$ trilayer and multilayer samples by dc magnetron sputtering onto Si(100) substrates. The general information has already been described elsewhere.[22] In this paper, we focused mainly on the process specific to CPP samples. A cryopump provided high pumping speeds with no oil vapor contamination and $<2\times10^{-7}$ Torr base pressure. The sputtering gas was ultrahigh purity Ar (99.999%) and was further purified by passage through a liquid N_2 cold trap to reduce impurities. Deposition was made under 1 mTorr Ar gas, and the temperature of the substrate was unregulated during fabrication of samples. For the deposition, 99.99% pure Co, Nb, and $Nb_{0.6}Ti_{0.4}$, and 99.97% $Nb_{0.4}Ti_{0.6}$ alloy targets were used as sources. The deposition rates were 0.7 nm/s for Co, 1.1 nm/s for Nb and $Nb_{0.6}Ti_{0.4}$, and 1.0 nm/s for $Nb_{0.4}Ti_{0.6}$, respectively.

To obtain comparable quality samples for different F and S layer thicknesses, up to eight different samples could be fabricated in the same run to minimize deviation in preparation conditions. The substrates were cleaned in acetone and a final ultrasonic rinse was performed in fresh alcohol. Nb and Co can form alloys at a high temperature, but they should be immiscible around room temperature.[23]

The sample design is illustrated in Fig. 1. The substrates were held in a circular stainless steel plate, which was located about 7 cm above the 2-in. sputtering sources. The CPP samples required three contact metal masks in different shapes.[24] A Nb strip was first deposited onto the substrate, followed by a circular electrode, the multilayer film of interest, a counterelectrode, and finally a top Nb strip, which is perpendicular to the first strip. Each strip was 200 nm thick in order to superconduct at 4.2 K. They could be both used as current and voltage leads. The masks in the sputtering system could be changed *in-situ*, so that the interfaces between the superconductor and ferromagnetic layers were not contaminated. The multilayer film of interest was sandwiched between circular superconducting electrodes to ensure equipotential surfaces at the top and bottom of the CPP sample, thus allowing uniform current through the whole sample regardless if the multilayer is normal or superconducting.

B. Measurement techniques

The CPP resistance measurement in metallic multilayer thin films is known to give fundamental information of the transport properties. For the study of giant magnetoresistance (GMR), the CPP resistance was analyzed by two-channel series resistance model to quantitatively separate the interface and bulk contributions.[25,26] In the F/S multilayers we study here, the current-in-plane (CIP) standard four-point measurement always gives zero resistance unless the samples were driven to normal state by warming, applying magnetic fields or currents larger than the critical values.

The small CPP resistance $R\approx10^{-8}\ \Omega$ of our samples was measured by a superconducting quantum interference device (SQUID) based picovolt meter.[27] The low noise dc currents were provided, up to 100 mA, from a battery-powered source. A small superconducting coil could produce a magnetic field (up to 800 Oe) in the layer plane, perpendicular to the current direction. At our measuring temperature of 4.2 K, the Nb strip and circular electrode remained superconducting, and thus ensured a uniform current distribution.

In the present experiment, the influence of the superconducting proximity effect on our CPP measurement was insignificant. Clearly, this effect arose from the presence of the Nb electrodes. If the sample was a nonmagnetic normal metal, the system may have become superconducting below some temperatures due to the reason that the Cooper pairs could penetrate from S into NM. For example, a 2.8 μm film of Ag beside Nb layer became superconducting at $\sim$1.6 K.[28] However, the ferromagnetic Co was able to stop the proximity effect effectively because of the pair-breaking effect in Co. Therefore, the bottom and the top of the multilayer were always Co films. Each sample had one bottom layer of Co plus N bilayers of Nb/Co, indicated as Co(d_{Co})/[Nb(d_{Nb})/Co(d_{Co})]$_N$.

We checked the structure of our multilayers with low angle and high angle θ-2θ x-ray scans. The high angle scans showed that Nb had bcc (110) structure and thicker Co had fcc (111) or hcp (0001), not distinguishable from θ-2θ scan. Our data confirmed that sputtered multilayers were polycrystalline. The total thickness of the CPP samples and the diameter W of circular electrode were checked with a stylus surface profiler. The deviation of thicknesses was found to be within 5% of the intended values. The small gap between the contact masks and the substrates resulted in rounded edge of the films. This edge effect contributes to the largest systematic error in this experiment. The uncertainty in the unit area

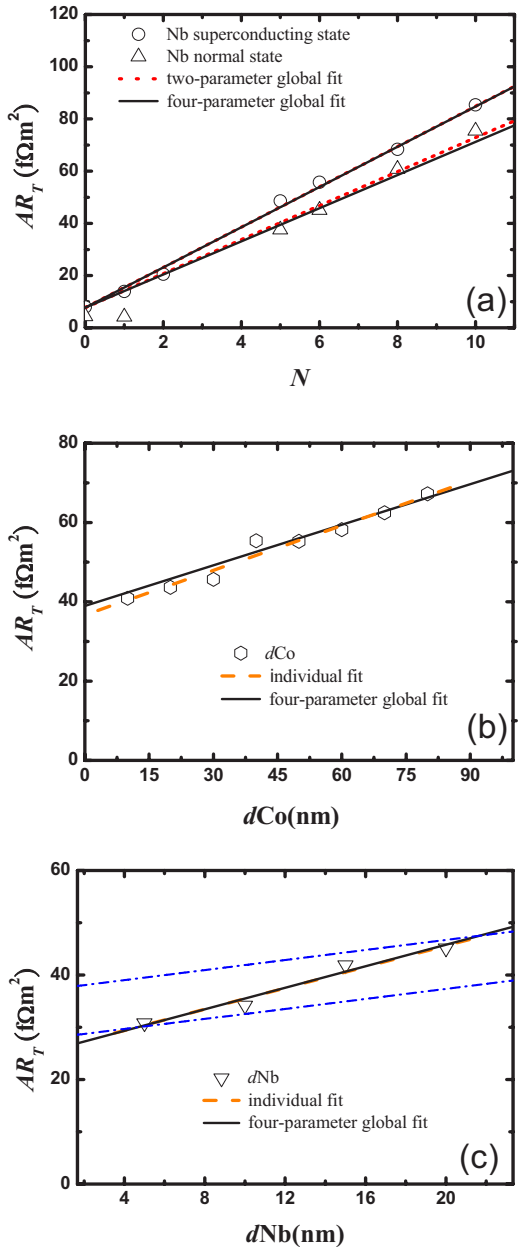

FIG. 2. (Color online) Data for Co/Nb multilayers. (a) Unit area resistance, AR_T, plotted against bilayer number N of two sets of samples with Nb thickness fixed at 20 nm and 80 nm, respectively. The dotted lines are fits for two parameters. (b) AR_T versus Co thickness with Nb thickness fixed at 20 nm and $N=6$. (c) AR_T versus Nb thickness with Co thickness fixed at 20 nm and $N=6$. The dashed lines are linear least square fits to individual sets. The dotted-dashed lines used the bulk CIP resistivities as the slope and the two interface resistances from two- and four-parameter fits as upper and lower limits, respectively. The solid lines in (a), (b), and (c) are global fits for four parameters to the data simultaneously.

total resistance AR_T of our multilayer samples was dominated by the uncertainty in $A=\pi(W/2)^2$, which is about 10% for the S samples and 15% for the NM samples.

III. RESULTS AND THE GLOBAL-FITTING PROCEDURE

Our sputtered bulk Nb films, no less than 500 nm thick, had a superconducting transition temperature $T_c \approx 9.2$ K. The resistivities of 500 nm Nb and Co films at 10 K were 8 and 7 $\mu\Omega$ cm, respectively, with an error of about 10%. From our previous results,[29] the T_c of the Nb/Co trilayers showed a monotonically rapid decrease with decreasing Nb thickness below 100 nm. Analyzing the experimental data within Radovic's model under the single mode approximation with high interface transparency, we derived the critical thickness $d_{\mathrm{Nb}}^{\mathrm{crit}} \approx 30$ nm, and the penetration depth $\xi_{\mathrm{FM}}^{\mathrm{Co}} \approx 1.2$ nm of the Cooper pair into the ferromagnetic layer. Below the $d_{\mathrm{Nb}}^{\mathrm{crit}}$, no superconducting transition was found down to 1.8 K. The large critical thickness $d_{\mathrm{Nb}}^{\mathrm{crit}}$ was due to the suppression of the superconducting wave function at the S/F interface by the pair-breaking effect from the strong exchange field E_{ex} in Co.

Four series of CPP samples were made for each S material. We shall use t to indicate that the thickness is fixed in the series of samples and d when the thickness is varied. For Nb, the series are

(1) Co(20)/[Nb(20)/Co(20)]$_N$ with t_{Nb} fixed at 20 nm ($<d_{\mathrm{Nb}}^{\mathrm{crit}}$) for normal state, t_{Co} fixed at 20 nm, and the numbers of bilayers were varied;
(2) Co(20)/[Nb(80)/Co(20)]$_N$ with t_{Nb} fixed at 80 nm ($>d_{\mathrm{Nb}}^{\mathrm{crit}}$) for superconducting state, t_{Co} fixed at 20 nm, and the numbers of bilayers were varied;
(3) Co(d_{Co})/[Nb(20)/Co(d_{Co})]$_6$ with t_{Nb} fixed at 20 nm, six bilayers, and varying Co thickness;
(4) Co(20)/[Nb(d_{Nb})/Co(20)]$_6$ with t_{Co} fixed at 20 nm, six bilayers, and varying Nb thickness but smaller than $d_{\mathrm{Nb}}^{\mathrm{crit}}$.

There was no giant magnetoresistance effect in Co/Nb multilayers with 20 nm or 80 nm of Nb thickness from our previous study.[24] The absence of giant magnetoresistance indicated that there was no spin memory across Nb layers. For Nb in NM state, bulk Nb was reported to have long spin-diffusion length. Strong spin mixing was present at the Nb/Cu interface.[30] Thus, our results suggest there is strong spin mixing at the Co/Nb interface. As the spin-up and spin-down electron channels could not be distinguished from the electric transport, we shall apply a one-band model to describe our CPP data. Each series of samples can be individually fitted with the model as the first way of analyzing our data. But results for the same quantity from different series can deviate. The second way is that we can apply the bulk resistivities of Nb and Co at 10 K to derive the two interface resistances as parameters from all series, as our previous results.[31] The third way is that we treat all resistivities and the interface resistances as fitting parameters to perform four-parameter global fit.

Figure 2(a) presents the plots of AR_T against bilayer number N for the first two series of samples. AR_T is linearly proportional to the number of bilayer for Nb both in normal and superconducting states. We can write out Eq. (1) and Eq. (2) explicitly for such linear behavior as

$$AR_T = 2AR_{F/S(S)} + \rho_F t_F + N(\rho_F t_F + \rho_S t_S + 2AR_{F/S(NM)}) \quad \text{for normal Nb,} \tag{1}$$

$$AR_T = 2AR_{F/S(S)} + \rho_F t_F + N(\rho_F t_F + 2AR_{F/S(S)}) \quad \text{for superconducting Nb.} \tag{2}$$

Here R_T is the measured total resistance of multilayers, t's

TABLE I. The derived values and parameters of different fitting procedures for the Co/Nb_xTi_{1-x} multilayers with $x=1$, 0.6, and 0.4.

	Co/Nb multilayer			
	ρ_{Co} ($\mu\Omega$ cm)	ρ_{Nb} ($\mu\Omega$ cm)	$2AR_S$ (fΩ m^2)	$2AR_{NM}$ (fΩ m^2)
Two parameter	7[a]	8[a]	6.3±0.9	3.5±0.7
Four parameter	4.9±0.6	17±2	6.7±0.3	1.9±0.5
	$Co/Nb_{0.4}Ti_{0.6}$ multilayer			
	ρ_{Co} ($\mu\Omega$ cm)	$\rho_{Nb0.4Ti0.6}$ ($\mu\Omega$ cm)	$2AR_S$ (fΩ m^2)	$2AR_{NM}$ (fΩ m^2)
Two parameter	7[a]	40[a]	9.9±0.7	2.3±1.9
Four parameter	7.2±0.4	50±6	9.9±0.2	1.4±0.5
	$Co/Nb_{0.6}Ti_{0.4}$ multilayer			
	ρ_{Co} ($\mu\Omega$ cm)	$\rho_{Nb0.6Ti0.4}$ ($\mu\Omega$ cm)	$2AR_S$ (fΩ m^2)	$2AR_{NM}$ (fΩ m^2)
Two parameter	7[a]	80[a]	22.6±1.7	5.6±1.5
Four parameter	6.5±0.6	102±7	22.9±0.2	2.1±0.7

[a]Bulk values measured in 500 nm thick films.

are the thicknesses, ρ's are the resistivities, and $AR_{F/S(NM),(S)}$'s are the interface resistances between normal state Nb and Co layers; and superconducting state Nb and Co layers, respectively. In our previously presented analysis of Nb/Co data, there is a mutual deviation using the individual fits. Thus, the two-parameter fitting procedure was executed because the two sets of data share the same parameter.[24] Using the bulk resistivities at 10 K for Co and normal Nb layers, we could extract $2AR_{Co/Nb(NM)}=3.5\pm0.7$ fΩ m^2 and $2AR_{Co/Nb(S)}=6.3\pm0.9$ fΩ m^2 from the slopes and interceptions of the y axis for data in Fig. 2(a). In the present analysis, we add two series of samples and then try whether we can perform global fitting procedure without using bulk resistivities (will be defined below). The resistivities will be determined by measuring the CPP resistance with varying layer thickness of Nb or Co.

Figures 2(b) and 2(c) show the AR_T behavior of the Co/Nb multilayers as functions of Co and Nb thickness, respectively, with d_{Nb} smaller than d_{Nb}^{crit} and $N=6$. The dashed lines show the individual fit results. The CPP resistance is linearly proportional to the thickness for both varied Co and Nb thickness ranges. With the one-band model, the linear behavior of AR_T versus thickness can be explicitly written as

$$AR_T = 2AR_{F/S(S)} + 12AR_{F/S(NM)} + 6\rho_S t_S + 7\rho_F d_F, \quad (3)$$

for varying Co thickness (d_F) with Nb thickness fixed at 20 nm and

$$AR_T = 2AR_{F/S(S)} + 12AR_{F/S(NM)} + 6\rho_S d_S + 7\rho_F t_F, \quad (4)$$

for varying Nb thickness (d_{Nb}) with Co thickness fixed at 20 nm. The individual linear least square fits of AR_T versus d_{Co} and d_{Nb} samples yield a slope ρ_{Co} of 5.4±0.4 $\mu\Omega$ cm and the other slope ρ_{Nb} of 17±2 $\mu\Omega$ cm, respectively. If we calculate interface resistance by setting the best fit values of resistivities from the slopes into Eq. (1) and Eq. (2), we find $AR_{Co/Nb(S)}=5.8\pm1.3$ fΩ m^2 and $AR_{Co/Nb(NM)}=3.4\pm1.2$ fΩ m^2 differing from the previously calculated values using bulk resistivities of Nb and Co. Therefore, we perform a four-parameter global fit to all the data simultaneously. The four parameters are $2AR_{Co/Nb(S)}$, $2AR_{Co/Nb(NM)}$, ρ_{Nb}, and ρ_{Co}. We can rewrite Eq. (1) as $AR_T=g_1+Ng_2+(N+1)t_{Co}g_3+Nt_{Nb}g_4$, Eq. (2) as $AR_T=(N+1)g_1+(N+1)t_{Co}g_3$, Eq. (3) as $AR_T=g_1+6g_2+7d_{Co}g_3+6t_{Nb}g_4$, and Eq. (4) as $AR_T=g_1+6g_2+7t_{Co}g_3+6d_{Nb}g_4$. Here g_1 is $2AR_{Co/Nb(S)}$, g_2 is $2AR_{Co/Nb(NM)}$, g_3 is ρ_{Co}, and g_4 is ρ_{Nb}. The solid lines in Figs. 2(a)–2(c) are global fits for four parameters to all the data simultaneously. We listed the best fit values in Table I. The interface resistance $2AR_{Co/Nb(S)}=6.7\pm0.9$ fΩ m^2 for pure Nb in the superconducting state is within the mutual experimental error of that reported by the Michigan State University group.[32]

The linear behavior of CPP resistance is reproduced when we use either $Nb_{0.4}Ti_{0.6}$ or $Nb_{0.6}Ti_{0.4}$ as a superconducting metal with $t_{Co}=20$ nm. The bulk resistivities at 10 K measured on sputtered single film of $Nb_{0.4}Ti_{0.6}$ and $Nb_{0.6}Ti_{0.4}$ were 40 $\mu\Omega$ cm and 80 $\mu\Omega$ cm, respectively, with errors of about 10%. The residual resistance ratios (RRR) were larger than 2 for Nb, ~1.25 for $Nb_{0.4}Ti_{0.6}$ and less than 1.06 for $Nb_{0.6}Ti_{0.4}$ films, indicating the quality of our $Nb_{0.6}Ti_{0.4}$ films is not as good as the others. The electron mean free paths estimated from these resistivities were 4.7 nm for pure Nb, 0.9 nm for $Nb_{0.4}Ti_{0.6}$, and 0.5 nm for $Nb_{0.6}Ti_{0.4}$ by assuming that the product $\langle\rho l\rangle=3.75\times10^{-6}$ $\mu\Omega$ cm^2 remained unchanged.[33,34] Moreover, the bulk Nb_xTi_{1-x} have $T_c=8.8$ and 7.0 K for $x=0.4$ and 0.6, respectively. When Nb_xTi_{1-x} films were sandwiched between Co, we also deduced $d_{Nb_{0.4}Ti_{0.6}}^{crit}\approx20$ nm and $d_{Nb_{0.6}Ti_{0.4}}^{crit}\approx27$ nm from fitting the T_c versus S thickness data to Radovic's model.[29,35] Detailed analysis will be presented elsewhere.[36] If S thickness was thinner than the critical value, we have NM/F multilayers, otherwise we have S/F multilayers. The S thickness in its

normal state for the first series of samples was kept at 8 nm for the smaller critical thicknesses. The linear AR_T versus the number of bilayers can be described by the two-parameter fit with Eq. (1) and Eq. (2). When bulk resistivities for Co and normal $Nb_{0.4}Ti_{0.6}$ were inserted, we obtained both the interface resistances as $Nb_{0.4}Ti_{0.6}$ is in the superconducting and normal state. The dotted lines in Fig. 3(a) represent these results. We also varied the Co and $Nb_{0.4}Ti_{0.6}$ thickness while the numbers of bilayers were fixed at six to treat CPP resistivities as fitting parameters to all data. These parameters, as shown in Table I, yielding the solid lines in Figs. 3(a)–3(c) provide a satisfactory prediction in comparison with data.

For the $Co/Nb_{0.6}Ti_{0.4}$ multilayers case, we obtain the interface resistances of $Co/Nb_{0.6}Ti_{0.4}$ in the normal state and in the superconducting state, as well as the CPP resistivities of Co and of $Nb_{0.6}Ti_{0.4}$ again from the two-parameter fit and four-parameter global fit. The best results of the calculations are shown as dotted lines for the two-parameter fit in Fig. 4(a), as dashed lines for individual fits for Figs. 4(b) and 4(c), and as solid lines for the four-parameter global fits. These parameters are summarized in Table I and the analysis of data will be discussed in Sec. IV. The interface resistance $2AR_{F/S(S)}=12.4\pm0.7$ fΩ m^2 for $Co/Nb_{0.5}Ti_{0.5}$ in the superconducting state was reported by the Michigan State University group with resistivity ~ 57 $\mu\Omega$ cm.[32] Our results scale with their numbers well.

IV. DATA ANALYSIS

In order to compare the interface and the bulk properties in the multilayers, we examine in the following two quantities, which are found in the literature as useful indicators. The relative contributions to CPP resistance can be found in the ratio between the interface resistance $R_{F/NM}$ and the bulk resistance in F within a spin-flip length l_{sf}^F or mean free path l. For $3d$ metals, the mean free path l is about 10 times shorter than the spin-flip length l_{sf}^F at low temperature.[37,38] To estimate the contribution of bulk resistance of the ferromagnet within its spin-active part, we choose l_{sf}^F instead of l. Thus, the quantity we are interested in is $\frac{R_{F/NM}}{R_{sf}^F}=\frac{AR_{F/S(NM)}}{\rho_{Co}l_{sf}^F}$ as described in the theoretical work of Ref. 39. The interface resistance $AR_{F/S(NM)}$ from our four-parameter fits are used in the following analysis. The spin-diffusion length was reported in Ref. 38 for electrodeposited Co, $l_{sf}^F=59\pm18$ nm at 77 K. The spin-diffusion length is an extrinsic quantity. It depends on the elastic mean free path and the spin-flip length. The spin-diffusion length should be larger in our case because our Co film has smaller resistivity and the measuring temperature was 4.2 K. Thus, we can calculate the upper limits $R_{F/NM}/R_{sf}^F\approx0.2$ for Nb/Co, $R_{F/NM}/R_{sf}^F\approx0.2$ for $Nb_{0.6}Ti_{0.4}$/Co, and $R_{F/NM}/R_{sf}^F\approx0.1$ for $Nb_{0.4}Ti_{0.6}$/Co, respectively. These ratios mean that the interface resistances are smaller than the relevant bulk resistances. The dominant contribution to the resistance comes from the bulk of Co, and with fair approximation to neglect the interface resistance with S in the normal state according to the theoretical work of Morten *et al.*[39]

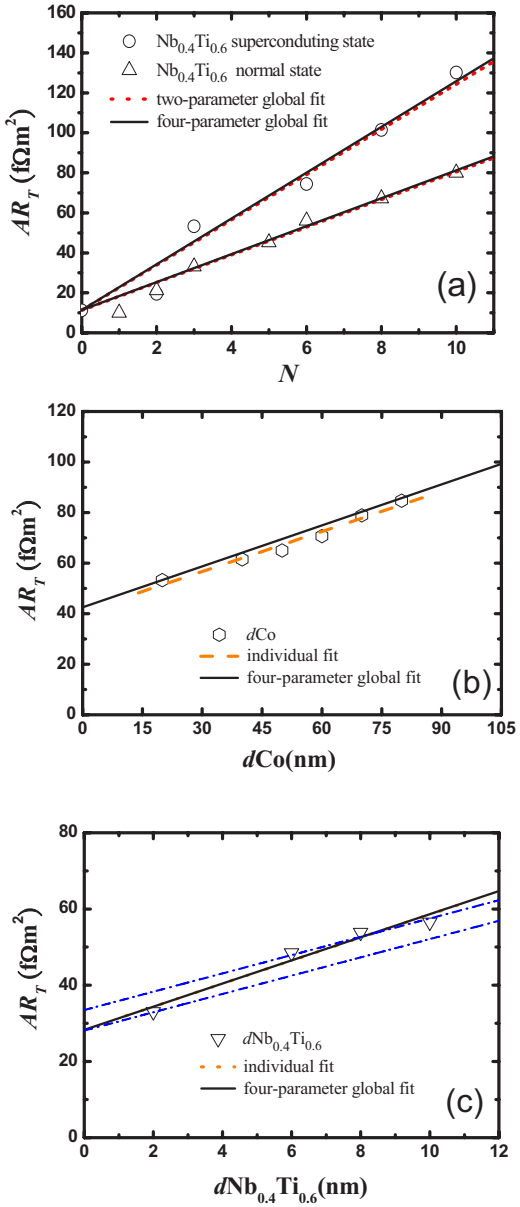

FIG. 3. (Color online) Data for $Co/Nb_{0.4}Ti_{0.6}$ multilayers. (a) Unit area resistance, AR_T, plotted against bilayer number N of two sets of samples with $Nb_{0.4}Ti_{0.6}$ thickness fixed at 8 nm and 80 nm, respectively. The dotted lines are fits for two parameters. (b) AR_T versus Co thickness with $Nb_{0.4}Ti_{0.6}$ thickness fixed at 8 nm and $N=6$. (c) AR_T versus $Nb_{0.4}Ti_{0.6}$ thickness with Co thickness fixed at 20 nm and $N=6$. The dashed lines are linear least square fits to individual sets. The dotted-dashed lines used the bulk CIP resistivities as the slope and the two interface resistances from two- and four-parameter fits as upper and lower limits, respectively. The solid lines in (a), (b), and (c) are global fits for four parameters to the data simultaneously.

However, the $AR_{F/S(S)}$ interface resistance is found to be larger than $AR_{F/S(NM)}$ and would give $R_{F/S}/R_{sf}^F>0.8$. When spin imbalance is taken into account near the interface, the increase in the CPP total resistance can be more dramatic if the NM region is taken to be a superconductor.[40] As shown in Figs. 1–3, the interface resistance $AR_{F/S(S)}$ with the super-

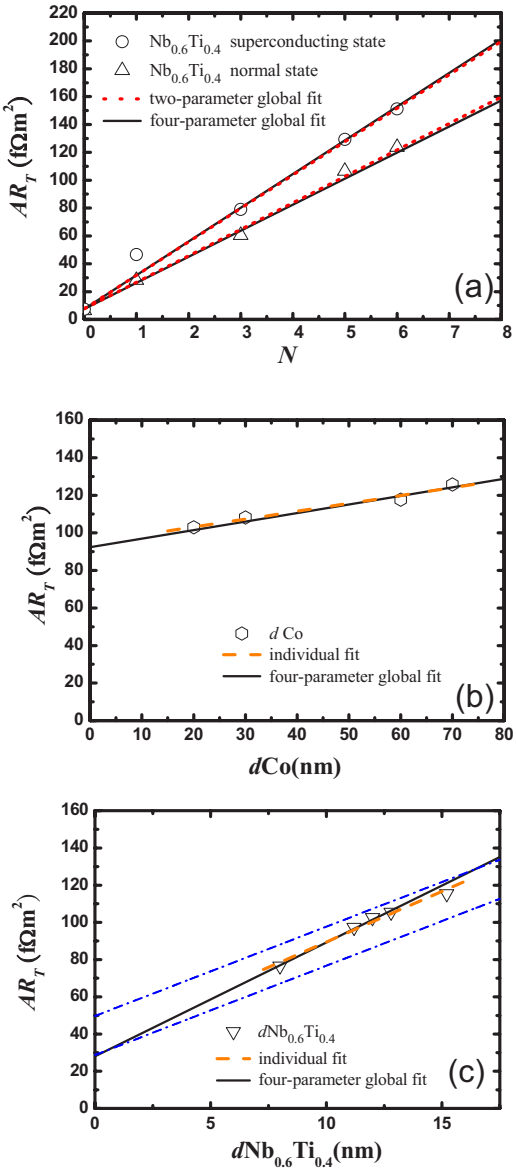

FIG. 4. (Color online) Data for $Co/Nb_{0.6}Ti_{0.4}$ multilayers. (a) Unit area resistance, AR_T, plotted against bilayer number N of two sets of samples with $Nb_{0.6}Ti_{0.4}$ thickness fixed at 15 nm and 80 nm, respectively. The dotted lines are fits for two parameters. (b) AR_T versus Co thickness with $Nb_{0.6}Ti_{0.4}$ thickness fixed at 15 nm and $N=6$. (c) AR_T versus $Nb_{0.6}Ti_{0.4}$ thickness with Co thickness fixed at 20 nm and $N=6$. The dashed lines are linear least square fits to individual sets. The dotted-dashed lines used the bulk CIP resistivities as the slope and the two interface resistances from two- and four-parameters fits as upper and lower limits, respectively. The solid lines in (a), (b), and (c) are global fits for four parameters to the data, simultaneously.

conductor in the superconducting state has a greater contribution to the total resistance. Therefore, the interface resistance of the F/S system is larger than that of the F/NM system with the materials we chose. The spin accumulation is a candidate for causing an additional voltage drop across the interface due to reduced spin transport into S. When spin-polarized current are injected onto the F/S interface from F, spin accumulation is established in the range of the spin-diffusion length in F. In S, the spin-polarized quasiparticle wave function decays because there are no available states. There are reports on conductance by subgap residual density of states and by crossed Andreev reflection.[41–43] However, the longest length scale for these phenomena can happen is the superconducting coherence length, ξ_S. Our S state samples have much larger thickness than ξ_S at the measuring temperature. In F, the spin accumulation decays because of spin-orbital scatterings. This causes an additional voltage drop associated with the interface. In the giant magnetoresistance effect in F/N multilayers, similar spin accumulation at the interface is responsible for the extra voltage drop.[44] It could be detected by a second F layer, which is parallel or antiparallel to the first one, placed within the spin-diffusion length of N. In our F/S multilayers, the S layers were much larger than the penetration length and we did not observe the spin-accumulation effect.

Our quantitative results clearly show that $R_{F/S}$ is larger than $R_{F/NM}$ in Co/Nb_xTi_{1-x} systems, where the S materials are in the dirty limit ($l<\xi_S$, see below). Electrons' wave functions decay exponentially when penetrating from a metal into a superconductor if their excitation energy with respect to the Fermi level is below the superconducting gap. In our CPP setup, the drop in voltage across the sample is at most 10 nanovolt for a maximum constant current of 100 mA, much smaller than the Nb energy gap $\Delta=1.76k_BT_c \sim 1.4$ meV. Current flows through the sample in response to a small applied voltage V less than Δ by means of the Andreev reflection. A spin-up electron from a normal metal is retroreflected at the interface as a spin-down hole in order to form a Cooper pair in the superconductor. This property makes a distinction between superconducting and normal states. The classical work of Blonder, Tinkham, and Klapwijk (BTK) (Ref. 45) described the Andreev reflection and the elastic scattering process at the N/S interface of a nanocontact. It interpolated between a perfect transparent interface and an insulating barrier at the interface with a barrier strength z varying from zero to infinity. The Andreev current at F/S interface is partially suppressed by the exchange splitting of the conduction band in the ferromagnet, which was demonstrated theoretically by de Jong and Beenakker.[46] To study the transport through N/S (Ref. 47) or F/S (Ref. 19) bilayers, the Usadel's equation was solved in the dirty limit. By considering the coherence length ξ_F in F metal, which is determined by exchange energy E_{ex}, the N/S bilayer can be easily adapted to the F/S case. In the general situation, the exchange energy is much larger than the superconducting gap, which makes ξ_F virtually independent of temperature. From the current continuity requirement, the boundary conditions for the anomalous Green's functions at interface were derived by Kuprianov and Lukichev.[48] The interface transparency parameter $\gamma_B=(AR_{F/S(NM)}/\rho_F\xi_F^*)$ is proportional to the interface resistance when superconductor is in the normal state. The boundary conditions are justified only when the exchange field in the F is much smaller than the Fermi energy. For strong F like Co in our case, appropriate boundary conditions for the Usadel's equations needs to be worked out.[2] Recently, the quasiclassical formalism, or the Eilenberger's equations, was employed for the Andreev conduc-

tance of N/S (Ref. 49) and F/S (Ref. 50) interfaces. Vodopyanov and Tagirov derived boundary conditions for the strong F case.[50] The quantum mechanical transmission and reflection coefficients for the two spin channels were discussed in the normal and superconducting states. However, the interface transparency was not taken into account.

Perfect transmission coefficient $T=1$ of the boundary conditions to the Usadel's equations was assumed in the work of Radovic *et al.*[6] Many experimental works on the F/S junctions in the CIP geometry applied the theory of Radoic *et al.* to explain the data. However, more and more reports pointed out that the inconsistency between data and calculation could be traced back to the assumption of continuity of the wave functions at the F/S interface. Analyses and procedures for fitting experimental results must take the finite transparency into account. For example, Aarts *et al.* were the first to observe the importance and presented experimental evidence of the intrinsically reduced interface transparency in the $V/V_{1-x}Fe_x$ multilayers.[21] They explained the nonmonotonic behavior in T_c as the competing effects of increasing attenuation depth ξ_F of the order parameter in the F material and the increasing transparency of the F/S interface for the penetration of Cooper pairs. Lazar *et al.* fitted their results on Fe/Pb/Fe trilayers by introducing interface transparency and noted its relation to the angular average of the transmission coefficient.[51] Kim *et al.*[17] reported the F layer thickness dependence of the T_c behaviors in bilayer F/S structures, determined by CIP resistance measurements. Quantitative analyses were made, the interface resistance at the Ni/Nb and $Cu_{0.4}Ni_{0.6}$/Nb boundary estimated from the best fit γ_B values were $2AR \sim 2.4$ fΩ m^2 for both Ni and $Cu_{0.4}Ni_{0.6}$. The estimated values are comparable to our CPP measurements with S in the normal state. Experimentally, γ_B is usually treated as an adjustable parameter to describe and modify the behavior of critical temperature dependence on the thickness for S or F.

We can estimate the interface transparency parameter γ_B without spin-flip scatterings directly from our results. The characteristic spatial scale is given by $\xi_F^*=\sqrt{\frac{\hbar D_F}{2\pi K_B T_C}}$, where $D_F=v_F l_F/3$ is the diffusion constant in F layer with the Fermi velocity v_F and the mean-free path l_F. Here, ξ_F^* is different from ξ_F^{ex} which corresponds to the actual penetration depth of the Cooper pairs in the F. While ξ_F^* is the Cooper-pairs penetration depth in normal metal without considering the exchange field. Both diffusion constant and ξ_F^{ex} of Co were derived to be $D_F=5$ cm^2/s and $\xi_F^{ex}=1.2$ nm from our previous evaluation.[29] These quantities allow us to obtain the following parameters in our F/S CPP multilayers: characteristic spatial length $\xi_F^* \approx 8.1$ nm and interface transparency parameter $\gamma_B \approx 1.7$ for Co/Nb, $\xi_F^* \approx 8.3$ nm, $\gamma_B \approx 1.2$ for $Co/Nb_{0.4}Ti_{0.6}$, and $\xi_F^* \approx 9.3$ nm, $\gamma_B \approx 1.6$ for $Co/Nb_{0.6}Ti_{0.4}$ when S is in the normal state. These finite transparency parameters justify the boundary conditions we used to describe the T_c dependence on S thicknesses with current parallel to the plane by using Radovic's model.[29,35] Numerical studies also showed insignificant discrepancy of the $T_c(d_S)$ behavior when using the boundary condition of high-quantum-mechanical transparency and of finite transparency introduced by Lazar *et al.*[51] and Tagirov.[4] For comparison, $\gamma_B=0.7$ for Ni/Nb bilayers,[17] and $\gamma_B=0.5$ and 1.15 in CoFe/Au and Au/Nb interface, respectively,[18] for CoFe/Au/Nb trilayers, were derived by fitting $T_c(d_F)$ curves. The given values for γ_B depend on the way by which ξ_F^* is calculated from the T_c. Experimentally, T_c in multilayers may be somewhat different from T_c in single films. We know that the transmission coefficient for the quasiparticles to form Cooper pairs in the F/S proximity effect theory is close to the smaller one between the transparency coefficients $T_\downarrow$ for spin-down and $T_\uparrow$ for spin-up electrons.[51,52] This is not the only mechanism since from our study the transparency can be varied by adjusting x as a result of changing compositional disorder or the changing lattice parameter between the Co and Nb_xTi_{1-x} interface. The spin-flip scattering is another mechanism which can lead to a large interface resistance. The interface spin-flips physically come from the following mechanisms: (1) inelastic electron scattering in the intermixed level between the magnetic and nonmagnetic layers; (2) the direction of magnetization changed locally near the interface; and (3) spin-orbit scattering at the interface induced by the polarization in magnetic layer. The spin-triplet symmetry can also be induced in a superconductor surrounded by ferromagnets with noncollinear magnetizations and spin-flip processes.[16,53] Thus, the value of interface resistance between the ferromagnet and the superconductor both in normal and superconducting states can provide a lot of physical information in F/S heterostructures.

Table I shows that the $Nb_{0.6}Ti_{0.4}$ had the largest resistivity in the normal state, and the largest interface resistance in both superconducting and normal states. According to Pippard's model[54] of partial quenching of Andreev reflection by impurities in the superconductor, the residual *NM/S* boundary resistance can be written as

$$AR = \frac{l_a}{2l_S}\rho_N l_N = \left(\frac{\rho_S l_a}{2\rho_S l_S}\right)(\rho_N l_N),$$

where $l_a=\hbar v_F/2\Delta=\pi\xi_S/2$ is the amplitude decay length in S for the electron evanescent mode from N, v_F is the Fermi velocity, Δ is the superconducting energy gap, ξ_S is the intrinsic coherence length, $\rho_0 l_0$ is the product of bulk resistivity ρ_0 and the mean free path l_0, and $\rho_S l_S$ is the product of ρ_S and l_S, when S is in the normal state just above T_c. Since $\rho l = m v_F/ne^2$ is a constant for each material, the equation shows that $AR_{NM/S}$ should be proportional to $\rho_S\xi_S$.[32] For the case of F/S interface, we can write the unit area conductance for two independent channels as $\frac{1}{AR_{\uparrow(\downarrow)}}=\frac{2l_S}{l_a}\frac{1}{\rho_{\uparrow(\downarrow)}l_{\uparrow(\downarrow)}}$. The sum of the two spin channel shows that the same relation holds and the Pippard model can be extended to ferromagnetic materials. The Ginsburg-Landau (GL) coherence length at zero temperature can be written as $\xi_{GL}(0)=\sqrt{\phi_0/2\pi s T_c}$, where $s=-dH_{c2}/dT$ close to T_c. We have deduced the $\xi_{Nb} \approx 12$ nm, $\xi_{Nb_{0.4}Ti_{0.6}} \sim 4$ nm, and $\xi_{Nb_{0.6}Ti_{0.4}} \sim 4.5$ nm from the temperature-dependent upper-critical-field measurements in previous works.[31] We find that the $AR_{F/S}$ derived from the two-parameter fit is indeed proportional to $\rho_S\xi_S$, which conformed very well to Pippard's model. The star symbol in Fig. 5 shows this linear relation between $AR_{F/S}$ and $\rho_S\xi_S$. Good agreement between our results and the theory suggests that

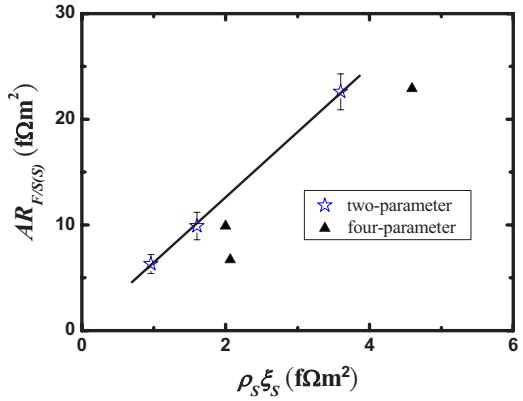

FIG. 5. (Color online) Unit area resistance, $AR_{F/S(S)}$, plotted against $\rho_S\xi_S$ for alloy Nb_xTi_{1-x} superconductor with $x=1$, 0.6, and 0.4. The solid line is linear least squares fit to the results of two-parameter fits.

the scattering centers and the penetration depths of the electron evanescent wave into the superconductors give rise to the interface resistance.

Although our two- and four-parameter fit resulted in different values of S resistivity, the $AR_{F/S(S)}$ values of our samples do not change much. The extracted interface resistances Co/Nb_xTi_{1-x} of our multilayers when the S materials are in their normal states are much larger than normal metal interface resistances such as Co/Cu and Co/Ag interfaces that had values ~ 0.5 fΩ m^2 or smaller.[25] Nb/Cu was reported to have large interface resistance of ~ 1 fΩ m^2.[30] Whether these large values are due to alloys at the interfaces or the crystalline mismatch (bcc for S to fcc or hcp for F)[55] remains to be investigated. However, the dependence of $AR_{F/S(S)}$ on $\rho_S\xi_S$ is inconsistent with a linear behavior using the values of $AR_{F/S}$ and ρ_S from the four-parameter global fit, as shown in Fig. 5. The CPP resistivity of Nb derived from the four-parameter global fit is more than 2 times larger than the CIP bulk value.

The CPP resistance in normal metal multilayers can be described by the theoretical work of Zhang and Levy.[56] For the CPP geometry, the current is constant throughout, while internal electric field varies from one layer to the next. In the CIP case, the voltage drop across the sample is the same but the current density in each layer is different. Zhang and Levy have shown that the CIP resistivity is an average of the conductivities $\rho_\parallel = L/\int_L \sigma_\parallel(z)dz$ while the CPP resistivity is the average of the resistivities $\rho_\perp = \int_L \rho_\perp(z)dz/L$, where L is the total thickness of the multilayers.[57] In other words, the total CPP resistance can be thought of as a series of different resistances of length d. The average of CPP resistivity removes the length scale by self-averaging. When the mean free path (l) is much larger than the thickness (d), the $\rho_\parallel$ and the $\rho_\perp$ are the same because the local conductivity is independent of position z. For large d/l they are quite different. Notice that when the scattering from the interface is much weaker than that from the bulk, $\rho_\perp$ is always greater than $\rho_\parallel$, because for the in-plane geometry the resistivity is dominated by the high conductivities layers. In our case, the thicknesses of normal Nb, $Nb_{0.6}Ti_{0.4}$, and $Nb_{0.4}Ti_{0.6}$ are between these two limit situations. The $\rho_\perp$ derived from the CPP measurements is larger than the $\rho_\parallel$ with parallel current.

The apparently large CPP resistivities for Nb and NbTi alloys derived in the four-parameter global fits could be explained by the fact that the interface resistance $AR_{F/S(NM)}$ is not constant when the superconductor is in the normal state. When layer thicknesses are systematically changed in the narrow window thinner than d_{Nb}^{crit}, thickness fluctuation might increase interface roughness in the thicker samples. By assuming a series resistance model, we attribute part of the extra interface resistance to the CPP resistivity. To verify this assumption, we plotted the dotted-dashed lines in Figs. 2, 3, and 4(c) with the bulk CIP resistivities as the slope and the two interface resistances from the two- and four-parameter fits as upper and lower limits, respectively. The thicknesses larger than l can be fitted by large $AR_{F/S(NM)}$ (Nb$>$4 nm, $Nb_{0.4}Ti_{0.6}$ and $Nb_{0.6}Ti_{0.4}>2$ nm), while thinner samples can be fitted by small $AR_{F/S(NM)}$. Thus, thickness fluctuation could be a possible explanation for the resistivities discrepancy, while the other NbTi alloys have less deviation. We can modify the global fit by assuming the $AR_{F/S(NM)}$ is linearly proportional to Nb (NbTi) thickness in the normal state and write $AR_{F/S(NM)}=a+bd_S$. The global fit becomes a five-parameter fit. But b and ρ_S become strongly dependent and cannot be determined independently. The small thickness range for Nb and NbTi being normal metals prevent us from more detailed studies of the thickness fluctuation. An appropriate model or more experimental data are needed. Another possible reason for the smaller AR values for thinner Nb (NbTi) samples is the presence of pin holes. The lack of interfaces through the pin holes makes the total resistance smaller. Even with the complication for ρ_S and $AR_{F/S(NM)}$, the influence on the extracted values of $AR_{F/S(S)}$ is small, as shown in Table I.

V. SUMMARY

We have presented the linear behavior of the CPP resistance in both normal and superconducting states of three different S materials in F/S multilayers. The best fits by the one-band model to normal and superconducting states data gave quantitative values of interface resistance. The normal state interface resistances are large. These direct measurements of the metallic interface resistance demonstrate that the interface transparency can be extracted and discussed quantitatively. We have also discussed the superconducting state interface resistance with the Pippard model. These analyses are important in understanding the transport properties between strong ferromagnets and superconductors in the diffusive regime.

ACKNOWLEDGMENTS

The authors would like to thank S. Yip for fruitful discussions, and W. T. Shi, W. L. Chang, and C. C. Huang for their help on some of the experiments. The financial support of the National Science Council (Contract No. NSC92-2112-M-001-053) and the Academia Sinica of Taiwan, Republic of China are acknowledged.

*Corresponding author. leesf@phys.sinica.edu.tw

[1] Yu. A. Izyumov, Yu. N. Proshin, and M. G. Khusainov, Phys. Usp. **45**, 109 (2002).
[2] A. I. Buzdin, Rev. Mod. Phys. **77**, 935 (2005).
[3] P. G. de Gennes, Rev. Mod. Phys. **36**, 225 (1964).
[4] L. R. Tagirov, Physica C **307**, 145 (1998).
[5] T. Kontos, M. Aprili, J. Lesueur, and X. Grison, Phys. Rev. Lett. **86**, 304 (2001).
[6] Z. Radović, M. Ledvij, L. Dobrosavljević-Grujić, A. I. Buzdin, and J. R. Clem, Phys. Rev. B **44**, 759 (1991).
[7] A. S. Sidorenko, V. I. Zdravkov, A. A. Prepelitsa, C. Helbig, Y. Luo, S. Gsell, M. Schreck, S. Klimm, S. Horn, L. R. Tagirov, and R. Tidecks, Ann. Phys. **12**, 37 (2003).
[8] J. S. Jiang, D. Davidović, D. H. Reich, and C. L. Chien, Phys. Rev. Lett. **74**, 314 (1995).
[9] Y. Obi, M. Ikebe, and H. Fujishiro, Phys. Rev. Lett. **94**, 057008 (2005).
[10] Y. Obi, M. Ikebe, T. Kubo, and H. Fujimori, Physica C **317**, 129 (1999).
[11] Th. Mühge, N. N. Garif'yanov, Yu. V. Goryunov, G. G. Khaliullin, L. R. Tagirov, K. Westerholt, I. A. Garifullin, and H. Zabel, Phys. Rev. Lett. **77**, 1857 (1996).
[12] V. V. Ryazanov, V. A. Oboznov, A. Yu. Rusanov, A. V. Veretennikov, A. A. Golubov, and J. Aarts, Phys. Rev. Lett. **86**, 2427 (2001).
[13] V. A. Oboznov, V. V. Bol'ginov, A. K. Feofanov, V. V. Ryazanov, and A. I. Buzdin, Phys. Rev. Lett. **96**, 197003 (2006).
[14] P. Fulde and R. A. Ferrel, Phys. Rev. **135**, A550 (1964).
[15] A. I. Larkin and Y. N. Ovchinnikov, Sov. Phys. JETP **20**, 762 (1965).
[16] H. Doh and H. Y. Choi, arXiv:cond-mat/0407149 (to be published).
[17] J. Kim, Jun Hyung Kwon, K. Char, and Hyeonjin Doh, Phys. Rev. B **72**, 014518 (2005).
[18] J. Kim, Y.-J. Doh, and K. Char, Phys. Rev. B **71**, 214519 (2005).
[19] Y. V. Fominov, N. M. Chtchelkatechev, and A. A. Golubov, Phys. Rev. B **66**, 014507 (2002).
[20] S. Reymond, P. SanGiorgio, M. R. Beasley, J. Kim, and J. Char, Phys. Rev. B **73**, 054505 (2004).
[21] J. Aarts, J. M. E. Geers, E. Bruck, A. A. Golubov, and R. Coehoorn, Phys. Rev. B **56**, 2779 (1997).
[22] S. F. Lee, C. Yu, W. T. Shih, Y. Liou, and Y. D. Yao, J. Magn. Magn. Mater. **209**, 231 (2000).
[23] R. Krishnan, J. Magn. Magn. Mater. **50**, 189 (1989).
[24] S. F. Lee, S. Y. Huang, J. H. Kuo, Y. A. Lin, and Y. D. Yao, J. Appl. Phys. **93**, 8212 (2003).
[25] J. Bass and W. P. Pratt, Jr., J. Magn. Magn. Mater. **200**, 274 (1999).
[26] T. Valet and A. Fert, Phys. Rev. B **48**, 7099 (1993).
[27] J. M. Slaughter, W. P. Pratt, Jr., and P. A. Schroeder, Rev. Sci. Instrum. **60**, 127 (1989).
[28] J. Slaughter, J. Bass, W. P. Pratt, Jr., P. A. Schroeder, and H. Sato, Jpn. J. Appl. Phys., Suppl. **26**, 1451 (1987).
[29] J. J. Liang, S. F. Lee, W. T. Shih, W. L. Chang, C. Yu, and Y. D. Yao, J. Appl. Phys. **92**, 2624 (2002).
[30] D. V. Baxter, S. D. Steenwyk, J. Bass, and W. P. Pratt, Jr., J. Appl. Phys. **85**, 4545 (1999).
[31] S. Y. Huang, S. F. Lee, J. C. Huang, G. H. Hwang, and Y. D. Yao, J. Appl. Phys. **97**, 10B103 (2005).
[32] C. Fierz, S. F. Lee, J. Bass, W. P. Pratt, Jr., and P. A. Schroeder, J. Phys.: Condens. Matter **2**, 9701 (1990).
[33] J. Bass, Landolt-Bornstein Numerical Data and Functional Relationships in Science and Technology, New Series, Group III, edited by K. H. Hellwege and J. L. Olsen (Springer, Berlin, 1982), Vol. 15a, p. 1.
[34] H. Weber, E. Seidl, C. Laa, E. Schachinger, M. Prohammer, A. Junod, and D. Eckert, Phys. Rev. B **44**, 7585 (1991).
[35] Z. Radović, L. Dobrosavljević-Grujić, A. I. Buzdin, and J. R. Clem, Phys. Rev. B **38**, 2388 (1988).
[36] S. F. Lee, S. Y. Huang, S. Y. Hsu, and Y. D. Yao (unpublished).
[37] M. Urech, V. Korenivski, and D. B. Haviland, J. Magn. Magn. Mater. **249**, 513 (2002).
[38] L. Piraux, S. Dubois, A. Fert, and L. Belliard, Eur. Phys. J. B **4**, 413 (1998).
[39] J. P. Morten, A. Brataas, and W. Belzis, Phys. Rev. B **72**, 014510 (2005).
[40] Igor Zutic, J. Fabian, and S. D. Sarma, Rev. Mod. Phys. **76**, 323 (2004).
[41] R. Mélin, Phys. Rev. B **73**, 174512 (2006).
[42] S. Russo, M. Kroug, T. M. Klapwijk, and A. F. Morpugo, Phys. Rev. Lett. **95**, 027002 (2005).
[43] D. Beckmann, H. B. Weber, and H. v. Löhneysen, Phys. Rev. Lett. **93**, 197003 (2004).
[44] T. Valet and A. Fert, Phys. Rev. B **48**, 7099 (1993).
[45] G. E. Blonder, M. Tinkham, and T. M. Klapwijk, Phys. Rev. B **25**, 4515 (1982).
[46] M. J. M. de Jone and C. W. J. Beenakker, Phys. Rev. Lett. **74**, 1657 (1995).
[47] S.-K. Yip, Phys. Rev. B **52**, 15504 (1995).
[48] M. Yu. Kuprianov and V. F. Lukichev, Sov. Phys. JETP **67**, 1163 (1988).
[49] S.-K. Yip, Superlattices Microstruct. **25**, 1213 (1999).
[50] B. P. Vodopyanov and L. R. Tagirov, JETP Lett. **77**, 126 (2003); **78**, 555 (2003).
[51] L. Lazar, K. Westerholt, H. Zabel, L. R. Tagirov, Yu. V. Goryunov, N. N. Garif'yanov, and I. A. Garifullin, Phys. Rev. B **61**, 3711 (2000).
[52] S. K. Upadhyay, A. Palanisami, R. N. Louie, and R. A. Buhrman, Phys. Rev. Lett. **81**, 3247 (1998).
[53] F. S. Bergeret, A. F. Volkov, and K. B. Efetov, Phys. Rev. B **69**, 174504 (2004).
[54] A. B. Pippard, Proc. R. Soc. London, Ser. A **391**, 255 (1984).
[55] C. Galinon, K. Tewolde, R. Loloee, W.-C. Chiang, S. Olson, H. Kurt, W. P. Pratt, Jr., J. Bass, P. X. Xu, Ke Xia, and M. Talanana, Appl. Phys. Lett. **86**, 182502 (2005).
[56] S. Zhang and P. M. Levy, J. Appl. Phys. **69**, 4786 (1991).
[57] S. Zhang and P. M. Levy, Phys. Rev. B **47**, 6776 (1993).